Quasi-geostrophic flow under location uncertainty

Long Li, Etienne Mémin, Bertrand Chapron

Quasi–geostrophic flow under location uncertainty

Long Li[1] Etienne Mémin[1] Bertrand Chapron[2]

[1]Inria/Irmar, Fluminance Group
Campus Universitaire de Beaulieu, 35042 Rennes Cedex, France

[2]Ifrmer, Laboratoire Spatial et Interfaces Air-Mer
Centre Bretagne, ZI de la Pointe du Diable, 29280 Plouzané, France

Outline

Location uncertainty (LU) principles

Stochastic flow

$$\mathrm{d}\boldsymbol{X}_t = \boldsymbol{u}(\boldsymbol{X}_t, t)\mathrm{d}t + \underbrace{\boldsymbol{\sigma}(\boldsymbol{X}_t, t)\mathrm{d}\boldsymbol{B}_t}_{\text{Uncertainty or Noise}} \tag{1}$$

Location uncertainty (LU) principles

Spatial structure of noise

- Correlation operator

$$\boldsymbol{\sigma}[\boldsymbol{f}](\boldsymbol{x},t) = \int_{\Omega} \breve{\boldsymbol{\sigma}}(\boldsymbol{x},\boldsymbol{y},t)\boldsymbol{f}(\boldsymbol{y})\mathrm{d}\boldsymbol{y} \tag{2}$$

$\breve{\boldsymbol{\sigma}}$ is assumed to be bounded

Location uncertainty (LU) principles

Spatial structure of noise

- Correlation operator

$$\boldsymbol{\sigma}[\boldsymbol{f}](\boldsymbol{x},t) = \int_{\Omega} \breve{\boldsymbol{\sigma}}(\boldsymbol{x},\boldsymbol{y},t)\boldsymbol{f}(\boldsymbol{y})\mathrm{d}\boldsymbol{y} \tag{2}$$

  $\breve{\boldsymbol{\sigma}}$ is assumed to be bounded

- Covariance and variance

$$\begin{aligned}\boldsymbol{Q}(\boldsymbol{x},\boldsymbol{y},t,s) &= \mathbb{E}\Big[\big(\boldsymbol{\sigma}(\boldsymbol{x},t)\mathrm{d}\boldsymbol{B}_t\big)\big(\boldsymbol{\sigma}(\boldsymbol{y},s)\mathrm{d}\boldsymbol{B}_s\big)^T\Big] \\ &= \delta(t-s)\mathrm{d}t\int_{\Omega}\breve{\boldsymbol{\sigma}}(\boldsymbol{x},\boldsymbol{z},t)\breve{\boldsymbol{\sigma}}^T(\boldsymbol{y},\boldsymbol{z},s)\mathrm{d}\boldsymbol{z} \qquad (3)\end{aligned}$$

$$\boldsymbol{a} \triangleq \boldsymbol{Q}/\mathrm{d}t = \boldsymbol{\sigma}\boldsymbol{\sigma}^T \tag{4}$$

Location uncertainty (LU) principles

Spectral representation

- Noise

$$\boldsymbol{\sigma}(\boldsymbol{x},t)\mathrm{d}\boldsymbol{B}_t = \sum_{n\in\mathbb{N}} \boldsymbol{\phi}_n(\boldsymbol{x},t)\mathrm{d}\beta_t^n \tag{5}$$

ϕ_n: orthogonal eigenfunctions of the covariance

β^n: 1D standard Brownian motions

Location uncertainty (LU) principles

Spectral representation

- Noise

$$\boldsymbol{\sigma}(\boldsymbol{x},t)\mathrm{d}\boldsymbol{B}_t = \sum_{n\in\mathbb{N}} \boldsymbol{\phi}_n(\boldsymbol{x},t)\mathrm{d}\beta_t^n \tag{5}$$

- Variance

$$\boldsymbol{a}(\boldsymbol{x},t) = \sum_{n\in\mathbb{N}} \boldsymbol{\phi}_n(\boldsymbol{x},t)\boldsymbol{\phi}_n^T(\boldsymbol{x},t) \tag{6}$$

ϕ_n: orthogonal eigenfunctions of the covariance

β^n: 1D standard Brownian motions

Location uncertainty (LU) principles

Stochastic Reynolds transport theorem (Mémin, 2014)

$$\mathrm{d}\int_{\mathcal{V}(t)}\theta(\boldsymbol{x},t)\mathrm{d}\boldsymbol{x}=\int_{\mathcal{V}(t)}(\mathrm{D}_t\theta+\theta\,\boldsymbol{\nabla}\cdot(\boldsymbol{u}-\boldsymbol{u}_s))\mathrm{d}\boldsymbol{x} \tag{7}$$

- Stochastic transport operator (Resseguier et al., 2017)

$$\mathrm{D}_t\theta\triangleq\mathrm{d}_t\theta+(\boldsymbol{u}-\boldsymbol{u}_s)\cdot\boldsymbol{\nabla}\,\theta\mathrm{d}t+\boldsymbol{\sigma}\mathrm{d}\boldsymbol{B}_t\cdot\boldsymbol{\nabla}\,\theta-\frac{1}{2}\,\boldsymbol{\nabla}\cdot(\boldsymbol{a}\boldsymbol{\nabla}\theta)\mathrm{d}t \tag{8}$$

Location uncertainty (LU) principles

Stochastic Reynolds transport theorem (Mémin, 2014)

$$\mathrm{d}\int_{\mathcal{V}(t)}\theta(\boldsymbol{x},t)\mathrm{d}\boldsymbol{x}=\int_{\mathcal{V}(t)}(\mathrm{D}_t\theta+\theta\,\boldsymbol{\nabla}\cdot(\boldsymbol{u}-\boldsymbol{u}_s))\mathrm{d}\boldsymbol{x} \tag{7}$$

- Stochastic transport operator (Resseguier et al., 2017)

$$\mathrm{D}_t\theta\triangleq\mathrm{d}_t\theta+(\boldsymbol{u}-\boldsymbol{u}_s)\cdot\boldsymbol{\nabla}\,\theta\mathrm{d}t+\boldsymbol{\sigma}\mathrm{d}\boldsymbol{B}_t\cdot\boldsymbol{\nabla}\,\theta-\frac{1}{2}\,\boldsymbol{\nabla}\cdot(\boldsymbol{a}\boldsymbol{\nabla}\theta)\mathrm{d}t \tag{8}$$

- Itô–Stokes drift (Bauer et al., 2020)

$$\boldsymbol{u}_s\triangleq\frac{1}{2}\,\boldsymbol{\nabla}\cdot\boldsymbol{a} \tag{9}$$

Location uncertainty (LU) principles

Transport under LU

- Conservation of extensive tracer

$$\mathrm{D}_t\theta = 0 \tag{10}$$

Location uncertainty (LU) principles

Transport under LU

- Conservation of extensive tracer

$$\mathrm{D}_t\theta = 0 \tag{10}$$

- Conservation of tracer energy (Resseguier et al., 2017)

$$\mathrm{d}_t \int_\Omega \frac{1}{2}\theta^2 \mathrm{d}\boldsymbol{x} = 0 \tag{11}$$

Outline

Barotropic quasi-geostrophic (QG) flow under LU

- Potential vorticity (PV)

$$q = \boldsymbol{\nabla} \times \boldsymbol{u} - \psi / R_d^2 + f \qquad \left(\boldsymbol{u} = \boldsymbol{\nabla}^{\perp} \psi\right) \tag{12}$$

Barotropic quasi-geostrophic (QG) flow under LU

- Potential vorticity (PV)

$$q = \boldsymbol{\nabla} \times \boldsymbol{u} - \psi / R_d^2 + f \qquad \left(\boldsymbol{u} = \boldsymbol{\nabla}^{\perp} \psi\right) \tag{12}$$

- Evolution of PV under LU

$$\mathrm{D}_t q = \left(\mathcal{D} + \mathcal{F}\right) \mathrm{d}t + \mathrm{d}\mathcal{S}_t^{\sigma} \tag{13}$$

Barotropic quasi-geostrophic (QG) flow under LU

- Potential vorticity (PV)

$$q = \boldsymbol{\nabla} \times \boldsymbol{u} - \psi/R_d^2 + f \qquad \left(\boldsymbol{u} = \boldsymbol{\nabla}^\perp \psi\right) \tag{12}$$

- Evolution of PV under LU

$$\mathrm{D}_t q = \left(\mathcal{D} + \mathcal{F}\right)\mathrm{d}t + \mathrm{d}\mathcal{S}_t^\sigma \tag{13}$$

- PV sources and sinks

$$\mathrm{d}\mathcal{S}_t^\sigma = \sum_i -\mathrm{J}\left(\sigma \mathrm{d}B_t^i - u_s^i \mathrm{d}t, u^i\right) + \frac{1}{2}\,\boldsymbol{\nabla}\cdot\left(\partial_i^\perp \boldsymbol{a} \boldsymbol{\nabla} u^i\right)\mathrm{d}t \tag{14}$$

J: Jacobi operator

Barotropic quasi-geostrophic (QG) flow under LU

- Potential vorticity (PV)

$$q = \boldsymbol{\nabla} \times \boldsymbol{u} - \psi/R_d^2 + f \qquad \left(\boldsymbol{u} = \boldsymbol{\nabla}^\perp \psi\right) \tag{12}$$

- Evolution of PV under LU

$$\mathrm{D}_t q = \big(\mathcal{D} + \mathcal{F}\big)\mathrm{d}t + \mathrm{d}\mathcal{S}_t^\sigma \tag{13}$$

- PV sources and sinks

$$\mathrm{d}\mathcal{S}_t^\sigma = \sum_i -\mathrm{J}\big(\sigma \mathrm{d}B_t^i - u_s^i \mathrm{d}t, u^i\big) + \frac{1}{2}\,\boldsymbol{\nabla}\cdot\big(\partial_i^\perp \boldsymbol{a} \boldsymbol{\nabla} u^i\big)\mathrm{d}t \tag{14}$$

  J: Jacobi operator

- Energy conservation $\left(\mathcal{D} = \mathcal{F} = 0\right)$ (Bauer et al., 2020)

$$\mathrm{d}_t \int_\Omega \frac{1}{2}\|\boldsymbol{\nabla}\psi\|^2 + \frac{1}{2}(\psi/R_d)^2 = 0 \tag{15}$$

Barotropic QG flow under LU

Test case: monochromatic Rossby wave

- Aim: study effect of small–scale inhomogeneity on structuration of large–scale flow

Barotropic QG flow under LU

Test case: monochromatic Rossby wave

- Aim: study effect of small–scale inhomogeneity on structuration of large–scale flow
- Configurations: initialized by a single Rossby wave; doubly periodic domain; under both homogeneous ($\boldsymbol{u}_s = 0$) and heterogeneous noise with same amplitude

Numerical results: effect of small–scale inhomogeneity

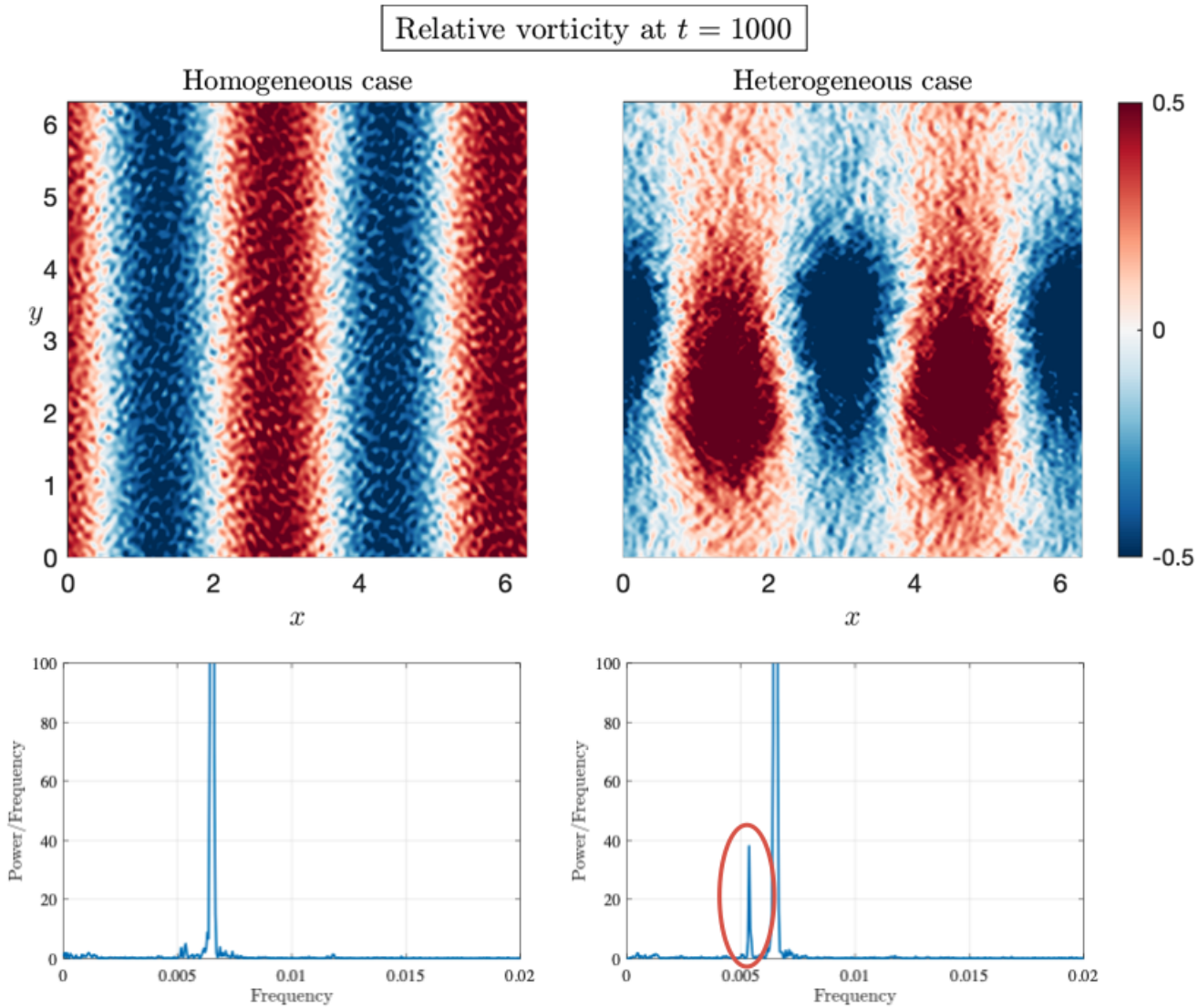

Click for video

Barotropic QG flow under LU

Test case: wind-driven circulation

- Aim: study low–frequency variability of LU coarse models

Barotropic QG flow under LU

Test case: wind-driven circulation

- Aim: study low–frequency variability of LU coarse models
- Configurations: double gyre wind forcing $\mathcal{F} = \frac{1}{f_0}\boldsymbol{\nabla} \times \boldsymbol{\tau}$; Biharmonic dissipation of vorticity $\mathcal{D} = -A_4 \nabla^6 \psi$; shallow basin ($R_d = \infty$) without topography; free–slip boundary condition; LU coarse model at 16×32, 32×64 and 64×128

Barotropic QG flow under LU

Test case: wind-driven circulation

- Aim: study low–frequency variability of LU coarse models
- Configurations: double gyre wind forcing $\mathcal{F} = \frac{1}{f_0}\boldsymbol{\nabla} \times \boldsymbol{\tau}$; Biharmonic dissipation of vorticity $\mathcal{D} = -A_4 \nabla^6 \psi$; shallow basin ($R_d = \infty$) without topography; free–slip boundary condition; LU coarse model at 16×32, 32×64 and 64×128
- POD noise

$$\boldsymbol{\sigma} \mathrm{d}\boldsymbol{B}_t = \sum_{n=N_1}^{N_2} \boldsymbol{\phi}_n \mathrm{d}\beta_t^n, \qquad \boldsymbol{a} = \sum_{n=N_1}^{N_2} \boldsymbol{\phi}_n \boldsymbol{\phi}_n^T \tag{16}$$

where the EOFs $\boldsymbol{\phi}_n$ are learned from eddy-resolving (256×512) data.

Numerical results: instantaneous variability

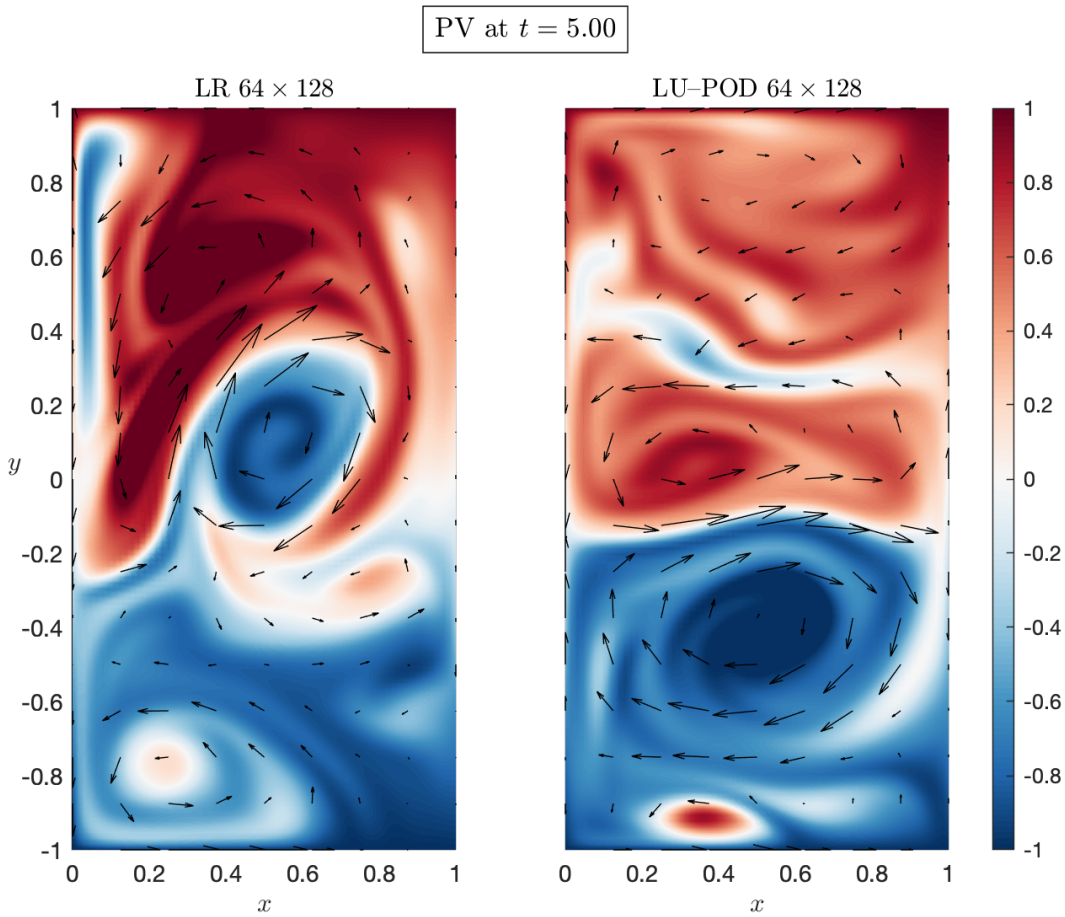

Click for video

Numerical results: qualitative accuracy of statistics

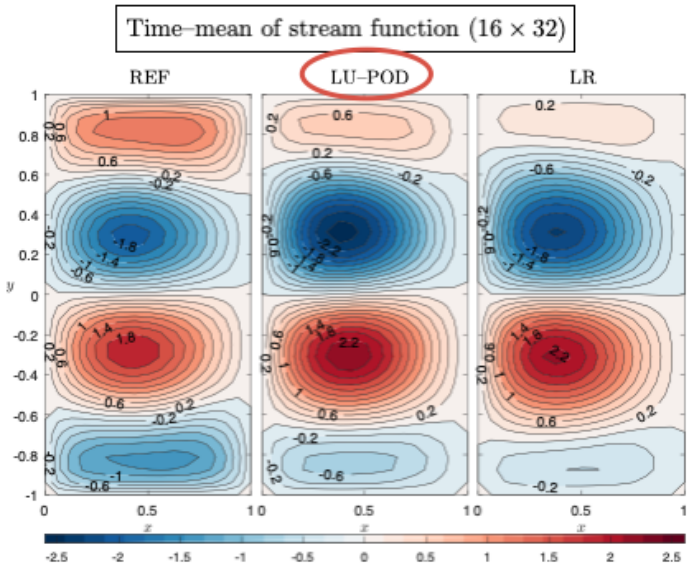

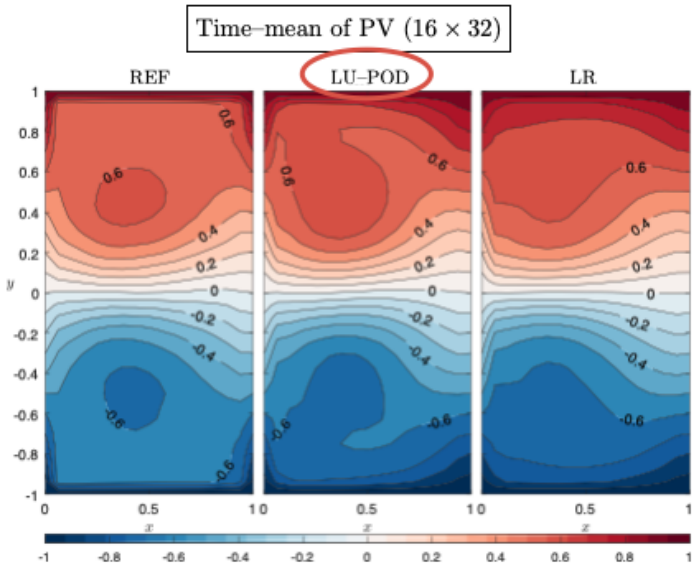

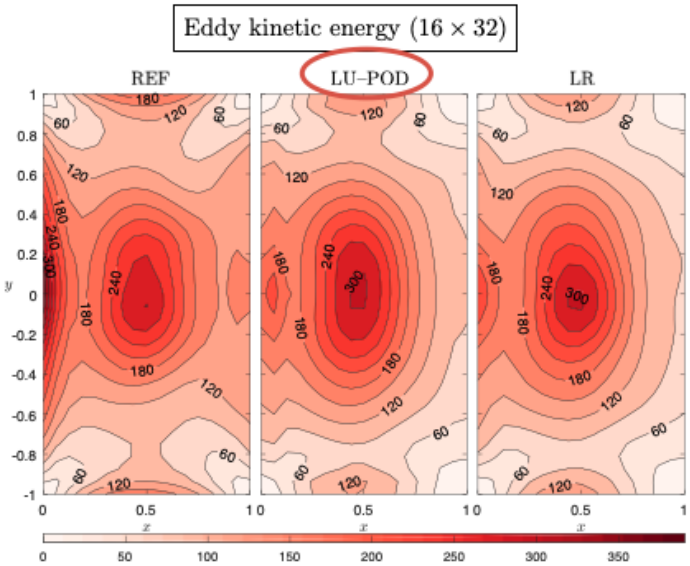

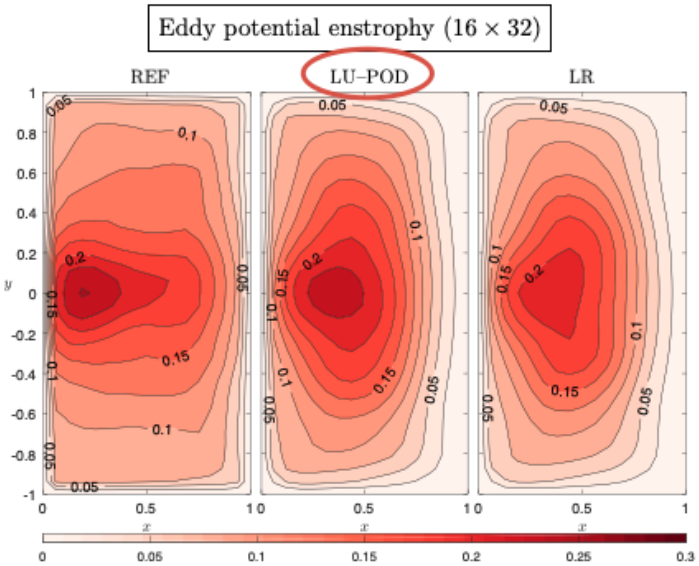

Numerical results: quantitative accuracy of statistics

Model	Mean	EKE	Skewness	Kurtosis
LR	0.108	0.073	0.190	0.218
LU	0.094	0.064	0.161	0.182
LU–NS	0.100	0.067	0.185	0.191
LU–CP	0.102	0.068	0.185	0.208

Table: Normalized RMSE of statistics for stream function (32×64)

Model	Mean	EKE	Skewness	Kurtosis
LR	0.061	0.122	0.166	0.155
LU	0.056	0.116	0.146	0.122
LU–NS	0.056	0.116	0.148	0.130
LU–CP	0.056	0.115	0.156	0.138

Table: Normalized RMSE of statistics for PV (32×64)

LU–NS: ~~$\boldsymbol{u}_s$~~

LU–CP: ~~$\boldsymbol{u}_s$~~ & ~~$\mathrm{d}\mathcal{S}_t^\sigma$~~

Numerical results: temporal behavior

Autocorrelation function for total circulation

$$\mathrm{ACF}(\tau) = \frac{1}{\sigma_\Psi^2} \overline{\left(\Psi(t) - \overline{\Psi}^t\right)\left(\Psi(t+\tau) - \overline{\Psi}^t\right)}^t, \tag{17}$$

where $\Psi(t) \triangleq \frac{1}{\Omega}\int_\Omega \psi(\boldsymbol{x}, t)\mathrm{d}\boldsymbol{x}$ with its standard derivation σ_Ψ.

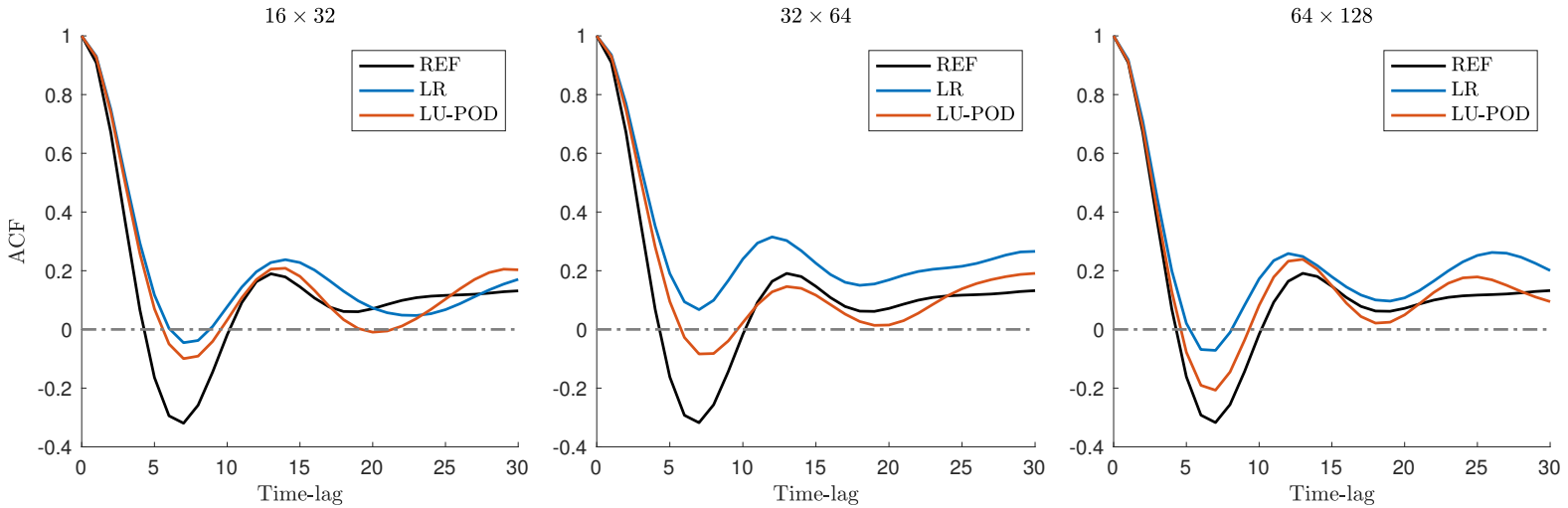

Outline

Multi–layered QG under LU

Quasi-geostrophic coupled model (Q–GCM) (Hogg et al., 2003)

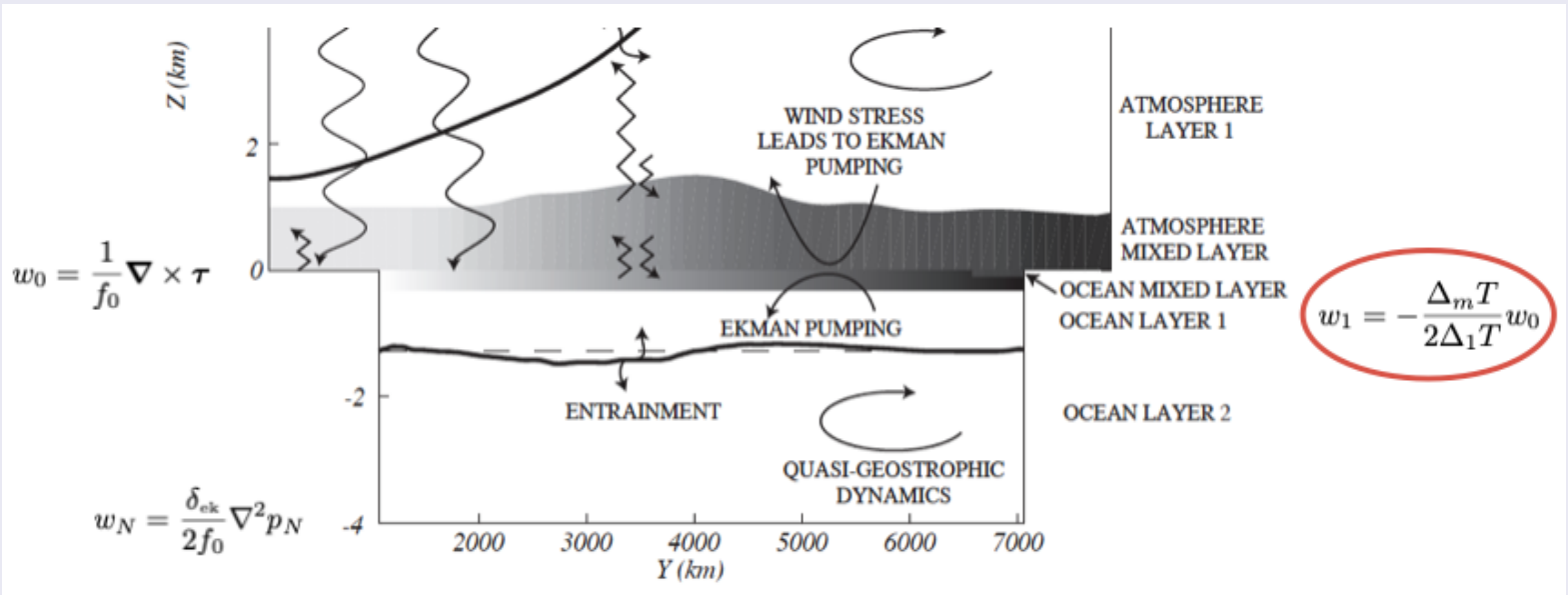

Quasi-geostrophic coupled model (Q–GCM) under LU

Governing equations

- Evolution of mixed–layer temperature

$$\mathrm{D}_t T_m = \big(\mathcal{D}_m + \mathcal{F}_m\big)\mathrm{d}t \tag{18}$$

Quasi-geostrophic coupled model (Q–GCM) under LU

Governing equations

- Evolution of mixed–layer temperature

$$\mathrm{D}_t T_m = \big(\mathcal{D}_m + \mathcal{F}_m\big)\mathrm{d}t \tag{18}$$

- Evolution of k–th layer PV

$$\mathrm{D}_t q_k = \big(\mathcal{D}_k + \mathcal{F}_k\big)\mathrm{d}t + \mathrm{d}\mathcal{S}^{\sigma}_{t,k}, \qquad \mathcal{F}_k = -\frac{f_0}{H_k}(w_k - w_{k-1}) \tag{19}$$

w: vertical entrainment

Quasi-geostrophic coupled model (Q–GCM) under LU

Governing equations

- Evolution of mixed–layer temperature

$$\mathrm{D}_t T_m = \big(\mathcal{D}_m + \mathcal{F}_m\big)\mathrm{d}t \tag{18}$$

- Evolution of k–th layer PV

$$\mathrm{D}_t q_k = \big(\mathcal{D}_k + \mathcal{F}_k\big)\mathrm{d}t + \mathrm{d}\mathcal{S}^{\sigma}_{t,k}, \qquad \mathcal{F}_k = -\frac{f_0}{H_k}(w_k - w_{k-1}) \tag{19}$$

w: vertical entrainment

- Evolution of k–th layer pressure

$$q_k = \frac{1}{f_0}\nabla^2 p_k + \frac{f_0}{H_k}(\eta_k - \eta_{k-1}) + \beta y \tag{20}$$

η: perturbed interface height

LU of type Gent–McWilliams (GM)

- Aim: constraint noise along "isopycnal" surfaces

$$\tilde{\boldsymbol{\sigma}}_k \mathrm{d}\boldsymbol{B}_t \perp \boldsymbol{\nabla}\Theta_k, \qquad \Theta_k \triangleq \frac{f_0}{H_k}(\eta_k - \eta_{k-1}) \tag{21}$$

LU of type Gent–McWilliams (GM)

- Aim: constraint noise along "isopycnal" surfaces

$$\tilde{\boldsymbol{\sigma}}_k \mathrm{d}\boldsymbol{B}_t \perp \boldsymbol{\nabla}\Theta_k, \qquad \Theta_k \triangleq \frac{f_0}{H_k}(\eta_k - \eta_{k-1}) \tag{21}$$

- Projected noise

$$\tilde{\boldsymbol{\sigma}}_k \mathrm{d}\boldsymbol{B}_t = \mathbf{P}_k(\boldsymbol{\sigma}_k \mathrm{d}\boldsymbol{B}_t), \qquad \mathbf{P}_k = \mathbf{I} - \frac{\boldsymbol{\nabla}\Theta_k(\boldsymbol{\nabla}\Theta_k)^T}{\|\boldsymbol{\nabla}\Theta_k\|^2} \tag{22}$$

LU of type Gent–McWilliams (GM)

- Aim: constraint noise along "isopycnal" surfaces

$$\tilde{\boldsymbol{\sigma}}_k \mathrm{d}\boldsymbol{B}_t \perp \boldsymbol{\nabla}\Theta_k, \qquad \Theta_k \triangleq \frac{f_0}{H_k}(\eta_k - \eta_{k-1}) \tag{21}$$

- Projected noise

$$\tilde{\boldsymbol{\sigma}}_k \mathrm{d}\boldsymbol{B}_t = \mathbf{P}_k(\boldsymbol{\sigma}_k \mathrm{d}\boldsymbol{B}_t), \qquad \mathbf{P}_k = \mathbf{I} - \frac{\boldsymbol{\nabla}\Theta_k(\boldsymbol{\nabla}\Theta_k)^T}{\|\boldsymbol{\nabla}\Theta_k\|^2} \tag{22}$$

- LU–GM diffusion tensor

$$\tilde{\boldsymbol{a}}_k = \mathbf{P}_k \boldsymbol{a}_k \mathbf{P}_k^T \tag{23}$$

Numerical results: instantaneous variability

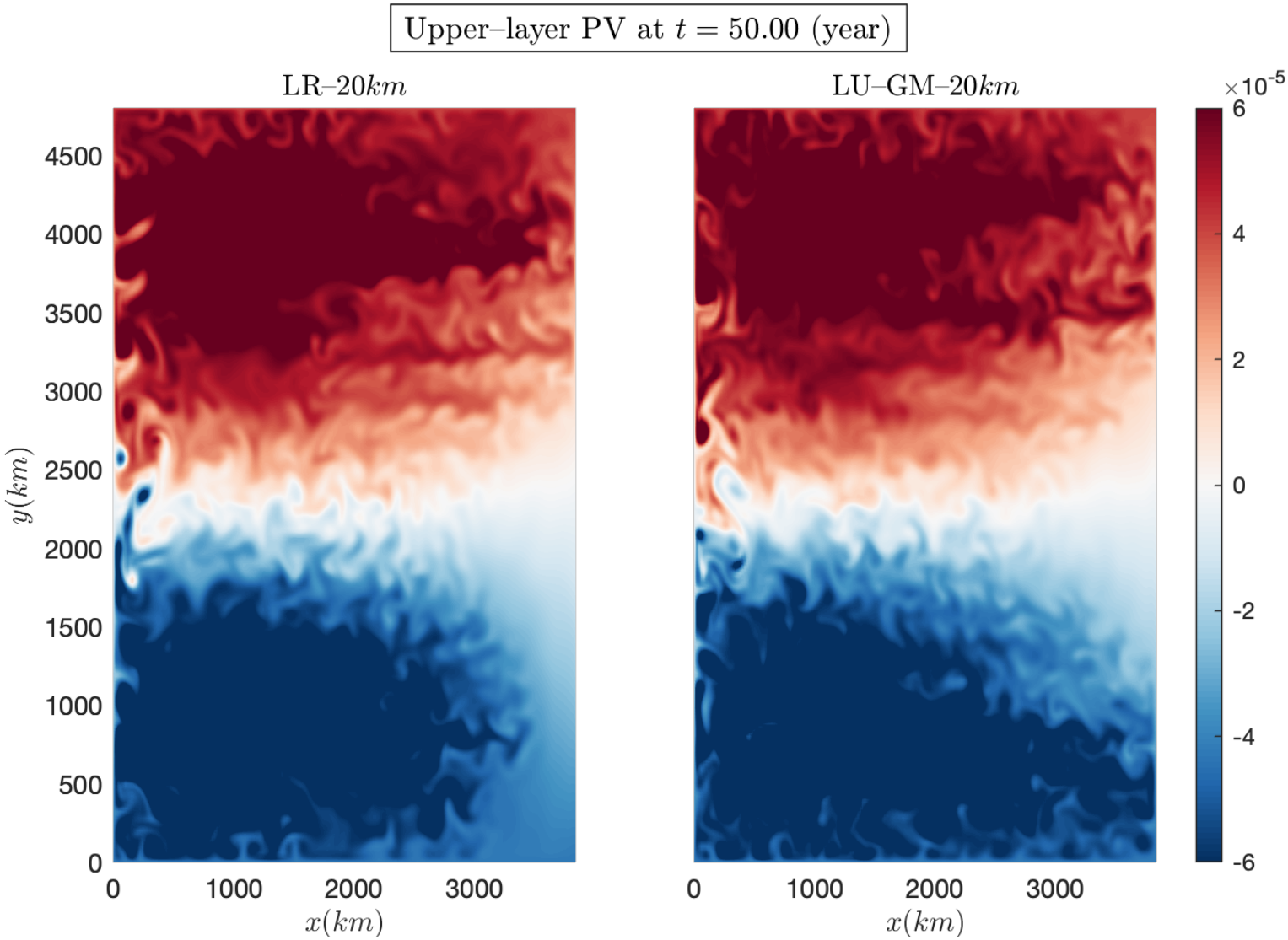

Click for video

Numerical results: instantaneous variability

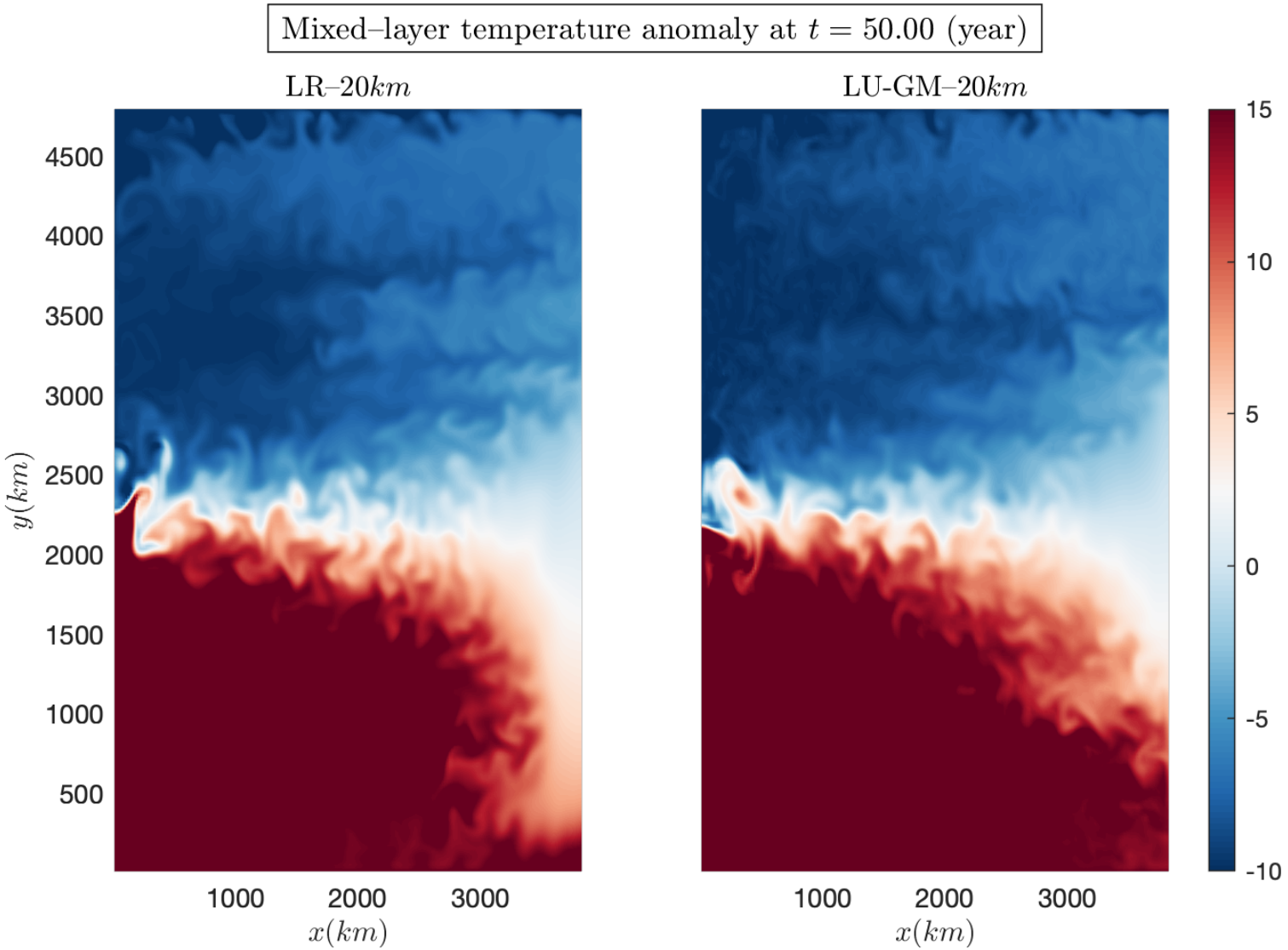

Click for video

Numerical results: low–frequency variability

Measures of statistics (Grooms et al., 2015)

- Pattern correlation (PC)

$$\mathrm{PC} = \frac{\int_\Omega \sigma_f^2 \sigma_{f_{\mathbf{ref}}}^2 \mathrm{d}\boldsymbol{x}}{(\int_\Omega \sigma_f^4 \mathrm{d}\boldsymbol{x})(\int_\Omega \sigma_{f_{\mathbf{ref}}}^4 \mathrm{d}\boldsymbol{x})} \quad \nearrow \tag{24}$$

Numerical results: low–frequency variability

Measures of statistics (Grooms et al., 2015)

- Pattern correlation (PC)

$$\text{PC} = \frac{\int_\Omega \sigma_f^2 \sigma_{f_{\textbf{ref}}}^2 \mathrm{d}\boldsymbol{x}}{(\int_\Omega \sigma_f^4 \mathrm{d}\boldsymbol{x})(\int_\Omega \sigma_{f_{\textbf{ref}}}^4 \mathrm{d}\boldsymbol{x})} \quad \nearrow \tag{24}$$

- Gaussian approximation of relative entropy

$$\text{Dispersion} = \frac{1}{|\Omega|} \int_\Omega \left(\frac{\sigma_{f_{\textbf{ref}}}^2}{\sigma_f^2} - 1 - \log\left(\frac{\sigma_{f_{\textbf{ref}}}^2}{\sigma_f^2} \right) \right) \mathrm{d}\boldsymbol{x} \quad \searrow \tag{25}$$

$$\text{Entropy} = \frac{1}{2} \left(\frac{1}{|\Omega|} \int_\Omega \frac{(\overline{f}^t - \overline{f}_{\textbf{ref}}^t)^2}{\sigma_f^2} \mathrm{d}\boldsymbol{x} + \text{Dispersion} \right) \quad \searrow \tag{26}$$

Numerical results: comparaison of measures

Model	RMSE of mean	RMSE of std	PC of std	Dispersion	Entropy
LR	0.41	0.71	0.51	79	41
LU–POD	0.38	0.69	0.52	38	19
LU–GM	0.36	0.66	0.53	16	8

Table: Measures of skill for upper–layer pressure ($40km$).

Model	RMSE of mean	RMSE of std	PC of std	Dispersion	Entropy
LR	0.23	0.64	0.51	194	98
LU–POD	0.22	0.62	0.56	72	36
LU–GM	0.22	0.58	0.64	24	12

Table: Measures of skill for middle–layer pressure ($40km$).

Model	RMSE of mean	RMSE of std	PC of std	Dispersion	Entropy
LR	0.12	0.67	0.57	1322	661
LU–POD	0.12	0.65	0.65	222	111
LU–GM	0.12	0.60	0.83	41	21

Table: Measures of skill for bottom–layer pressure ($40km$).

Numerical results: comparaison of measures

Model	RMSE of mean	RMSE of std	PC of std	Dispersion	Entropy
LR	0.44	0.71	0.44	851	26
LU–POD	0.44	0.69	0.46	36	18
LU–GM	0.41	0.66	0.50	15	8

Table: Measures of skill for upper–layer pressure ($80km$).

Model	RMSE of mean	RMSE of std	PC of std	Dispersion	Entropy
LR	0.26	0.60	0.58	188	94
LU–POD	0.26	0.59	0.61	67	34
LU–GM	0.25	0.55	0.70	18	9

Table: Measures of skill for middle–layer pressure ($80km$).

Model	RMSE of mean	RMSE of std	PC of std	Dispersion	Entropy
LR	0.12	0.67	0.56	1701	851
LU–POD	0.12	0.65	0.65	248	124
LU–GM	0.12	0.59	0.80	40	20

Table: Measures of skill for bottom–layer pressure ($80km$).

Numerical results: low–frequency variability

Energy pathways (Hogg and Blundell, 2006)

- KE decomposition

$$\mathrm{KE}_k = \frac{\rho H_k}{2}\Big(\underbrace{\langle u_k \rangle^2}_{\text{Zonal KE}} + \underbrace{\left(\overline{u_k}^2 + \overline{v_k}^2\right)}_{\text{Standing EKE}} + \underbrace{\left(u_k'^2 + v_k'^2\right)}_{\text{Transient EKE}} \Big) \tag{27}$$

Numerical results: (eddy) kinetic energy budget

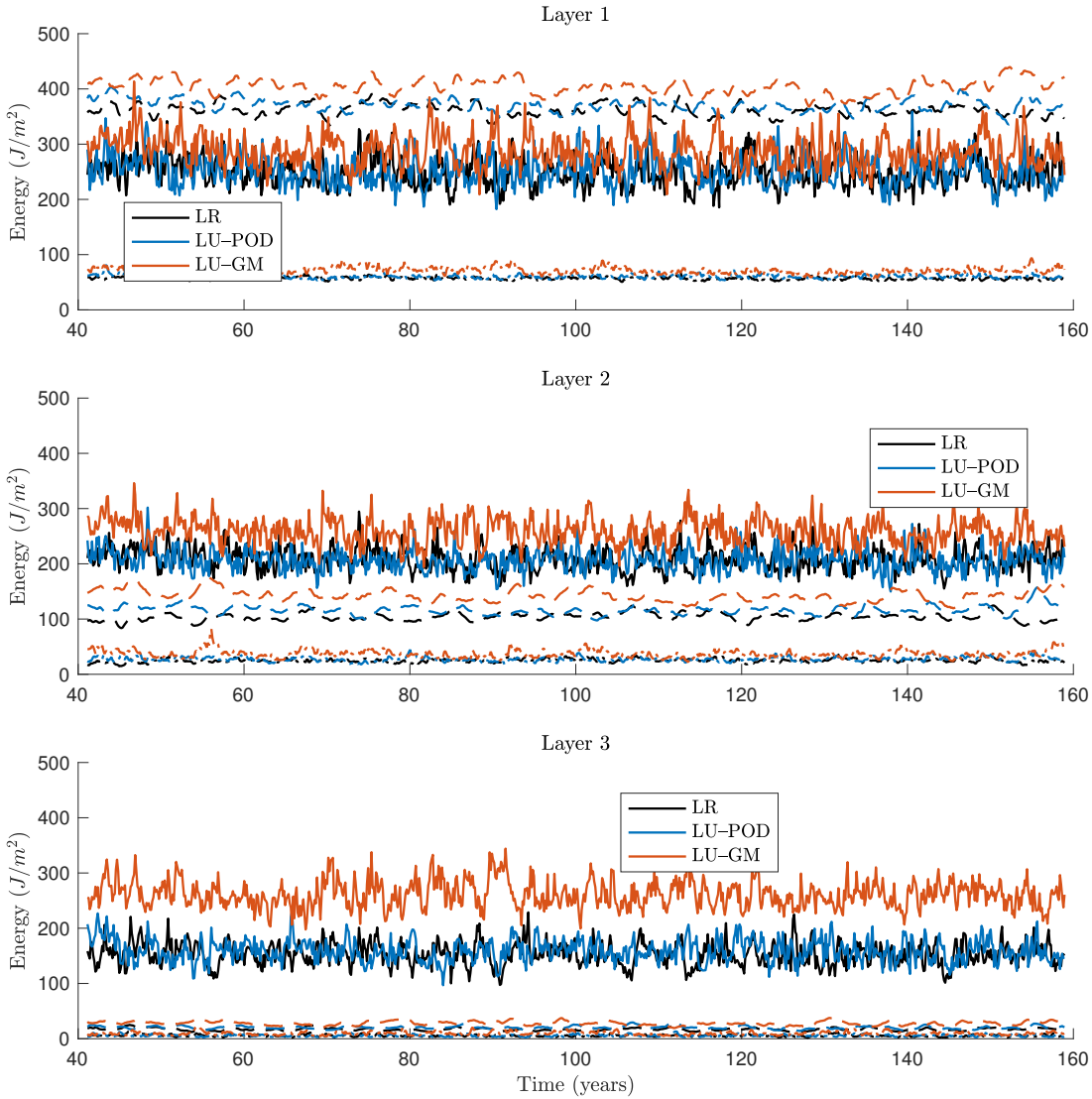

Figure: Comparaison of zonal (dotted lines), standing eddy (dashed lines), and transient eddy kinetic energy (solid lines), for different coarse ($40km$) models, in (a) layer 1, (b) layer 2, and (c) layer 3.

Numerical results: energy exchange

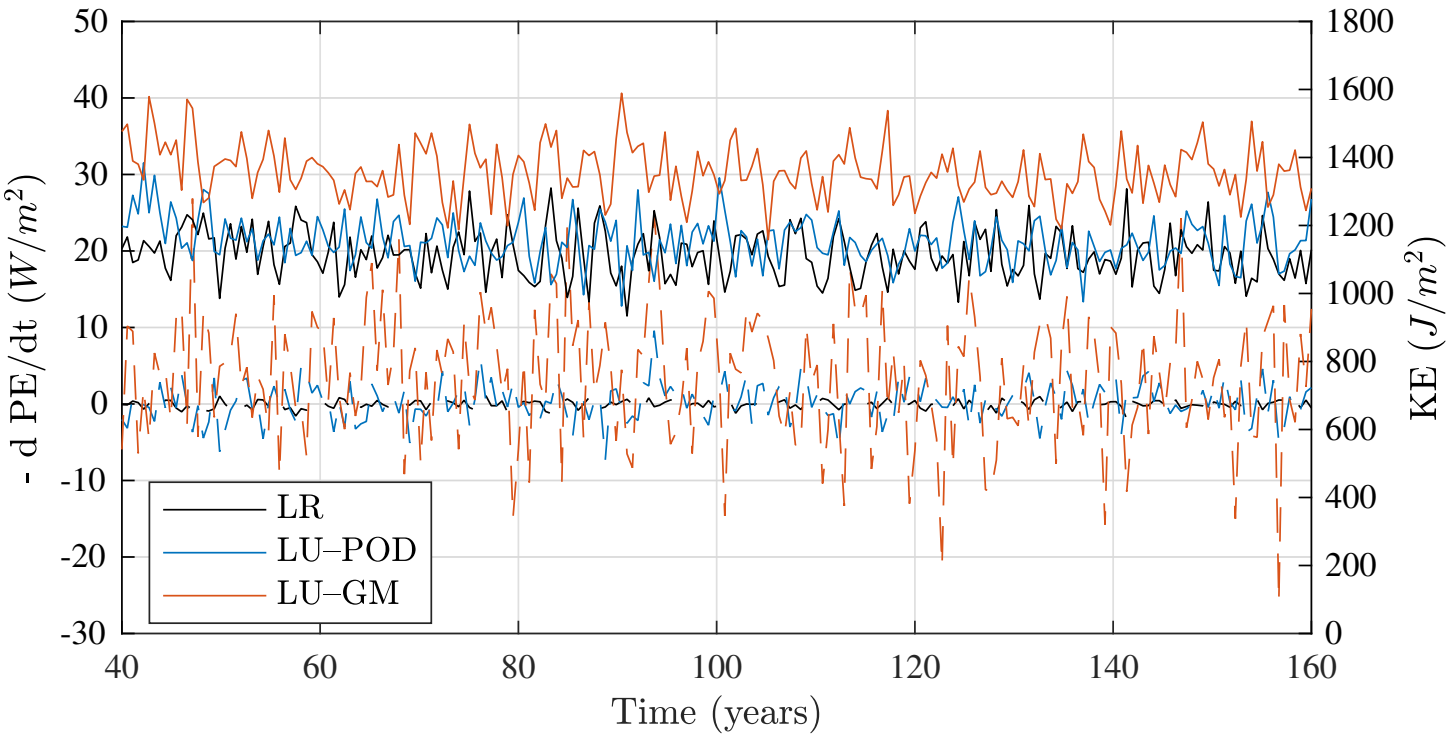

Figure: Time series of the negative rate of change of potential energy (dashed lines) and total kinetic energy (solid lines), for different coarse ($40km$) models.

Future works

- Development of jets

Future works

- Development of jets
- LU eddy–resolving simulation ($\sim 10km$)

Future works

- Development of jets
- LU eddy–resolving simulation ($\sim 10km$)
- Southern channel ocean (Hogg and Blundell, 2006)

Future works

- Development of jets
- LU eddy–resolving simulation ($\sim 10km$)
- Southern channel ocean (Hogg and Blundell, 2006)
- Atmosphere–ocean coupled mode (Hogg et al., 2003)

Future works

- Development of jets
- LU eddy–resolving simulation ($\sim 10km$)
- Southern channel ocean (Hogg and Blundell, 2006)
- Atmosphere–ocean coupled mode (Hogg et al., 2003)
- Multiple scale ocean model (combines planetary and quasi–geostrophic physics) (eg. MSQG)

Future works

- Development of jets
- LU eddy–resolving simulation ($\sim 10km$)
- Southern channel ocean (Hogg and Blundell, 2006)
- Atmosphere–ocean coupled mode (Hogg et al., 2003)
- Multiple scale ocean model (combines planetary and quasi–geostrophic physics) (eg. MSQG)
- Implement LU–GM in primitive model (eg. NEMO)

Future works

- Development of jets
- LU eddy–resolving simulation ($\sim 10km$)
- Southern channel ocean (Hogg and Blundell, 2006)
- Atmosphere–ocean coupled mode (Hogg et al., 2003)
- Multiple scale ocean model (combines planetary and quasi–geostrophic physics) (eg. MSQG)
- Implement LU–GM in primitive model (eg. NEMO)
- Application to ensemble data assimilation (Cotter et al., 2020)

Thank for Your Attention!

References

W. Bauer, P. Chandramouli, B. Chapron, L. Li, and E. Mémin. Deciphering the role of small-scale inhomogeneity on geophysical flow structuration: a stochastic approach. *Journal of Physical Oceanography*, 50(4):983–1003, 2020.

C. Cotter, D. Crisan, D. D. Holm, W. Pan, and I. Shevchenko. Data assimilation for a quasi-geostrophic model with circulation-preserving stochastic transport noise. *Journal of Statiscal Physics*, 2020.

I. Grooms, A. J. Majda, and K. S. Smith. Stochastic superparameterization in a quasigeostrophic model of the Antarctic Circumpolar Current. *Ocean Modelling*, 85: 1–15, 2015.

A. McC. Hogg and J. R. Blundell. Interdecadal variability of the southern ocean. *Journal of Physical Oceanography*, 36:1626–1645, 2006.

A. McC. Hogg, W. K. Dewar, P. D. Killworth, and J. R. Blundell. A quasi-geostrophic coupled model (Q-GCM). *Monthly Weather Review*, 131(10):2261–2278, 2003.

E. Mémin. Fluid flow dynamics under location uncertainty. *Geophysical & Astrophysical Fluid Dynamics*, 108(2):119–146, 2014.

V. Resseguier, E. Mémin, and B. Chapron. Geophysical flows under location uncertainty, part I: Random transport and general models. *Geophysical & Astrophysical Fluid Dynamics*, 111(3):149–176, 2017.